International Journal of Heat and Technology
Vol. 36, No. 2, June, 2018, pp. 687-696
Journal homepage: http://iieta.org/Journals/IJHT

Numerical simulation of pressure waves induced by high-speed maglev trains passing through tunnels

Yongxing Jia, Yuangui Mei*

Lanzhou Jiaotong University, Gansu Province Engineering Laboratory of Rail Transit Mechanics Application, Lanzhou 730070, China

Corresponding Author Email: meiyuangui@163.com

https://doi.org/10.18280/ijht.360234

Received: 5 October 2017
Accepted: 23 February 2018

Keywords:
high-speed maglev train, numerical simulation, method of characteristics, pressure wave, tunnel

ABSTRACT

This paper aims to determine the proper cross-sectional area for tunnels on high-speed maglev lines and support the optimization of the airtightness design for high-speed maglev trains. For these purposes, the pressure fluctuations in the tunnel operation of two maglev trains with the speed up to 650km/h were simulated using the 1D compressible unsteady non-homentropic flow model and the method of characteristics. The simulation results were compared to those from the reduced-scale test in Japan and full-scale test in China. The comparison proves that our 1D model is a rational and efficient tool for pressure wave prediction. Through repeated computations of the 1D model, the critical tunnel lengths were obtained. Then, the effects of tunnel length, tunnel cross-sectional area, train speed and train length on maximum pressure variation were identified one by one. The research findings provide a valuable reference for the tunnel and train design on high-speed maglev lines.

1. INTRODUCTION

At present, there are two typical technical routes for the development of high-speed maglev, namely, the high-temperature superconducting magnetic levitation in Japan and the room-temperature superconductivity magnetic levitation in German. The only commercially-operated high-speed maglev line is the Shanghai Transrapid, which operates at the maximum speed of 431 km/h. The TR-09 manned maglev train reached 550 km/h in speed tests. Meanwhile, the Japanese superconducting maglev train hit 603 km/h on the Yamanashi Test Line. It is clear that high-speed maglev train greatly surpasses conventional wheel-rail high-speed train in operation speed. However, this advantage comes at the expense of strict aerodynamic requirements on the train, especially in tunnel operations. When a high-speed maglev train passes through a tunnel, there will be severe pressure fluctuations in the tunnel, leading to aural discomfort of passengers, fatigue damage of the train and its components, and safety accidents to tunnel equipment and workers. Therefore, it is very meaningful to make accurate predictions of the pressure wave generated during the tunnel operation of high-speed maglev trains.

Numerous studies have explored the pressure wave caused by high-speed trains passing through the tunnel. However, there are relatively few reports on the pressure wave in tunnel induced by high-speed maglev trains. Since 1977, Japanese scholars have investigated various aerodynamic problems of high-speed maglev trains on the Miyazaki Test Line and the Yamanashi Test Line. For instance, Masahiro Sugesawa et al. [1] conducted a full-scale test on the aerodynamics of MLX01 test train, such as surface pressure, rear-end flow separation, air resistance, micro-pressure waves, and the interior/exterior noise features. Through full-scale and reduced-scale tests, Kazuya Takahashi [2] and Atsushi Honda [3-4] examined the features of the micro-pressure wave and the performance of the tunnel buffer structure when a maglev train passes through the tunnel. Saito Tsutoshi [5] identified the relationship between initial compression wave and micro-pressure wave during the tunnel operation of high-speed maglev trains. Focusing on tunnel pressure waves, Mikio Yamazaki et al. [6-7] employed full-scale test and computational fluid dynamics (CFD) to investigate the pressure fluctuations caused by a 3-car group MX01 train passing through a 4km-long tunnel at the speed of 500 km/h. Through shallow water-table, Kazuya Kikawada et al. [8] concluded that the pressure change is 9kPa at the centre of a 1,445 m-long tunnel if only one train passes through the tunnel at 500 km/h at the blockage ratio of 0.130, and 18 kPa if two trains pass through the tunnel under the same conditions.

Owing to the lack of tunnels in the Emsland test facility and the Shanghai Transrapid, German and Chinese scholars have only theoretically analysed the pressure wave caused by high-speed maglev trains passing through the tunnel. Under the outside maximum pressure threshold of 5.5 kPa, Th. Tielkes [9] compared the aerodynamics of traditional intercity express (ICE) trains and maglev trains, and recommended the dynamic airtightness index of 20 s and the tunnel cross-sectional areas of 72, 95, 123 and 156 m^2, respectively for 300, 350, 400, and 450 km/h trains. Zhang Guangpeng et al. [10] studied the effect of operating speed and tunnel length on the pressure wave caused by the tunnel operation of a TR-type maglev train, and gave recommended tunnel cross-sectional area according to Germany and ERRI pressure comfort criterions. Zhang Zhaojie [11] used CFD method to determine the pressure wave features of a 250 km/h maglev train based on the secondary development of FLUENT. Liu Chaoqun et al. [12] compared the internal profile of the tunnels around the world with TR08 maglev train passing at 350 km/h, 400 km/h and 450 km/h, but failed to make a systematic calculation or analysis. Reference

[23] establishes pressure calculation methods and procedures for single- and double-train tunnel operations based on non-homentropic flow model [23]. Mei Yuangui [20] conducted in-depth research on the pressure wave of high-speed train tunnels for many years.

Full-scale test is the best way to obtain the exact pressure features in the tunnel operation of high-speed maglev trains. However, such a test is not suitable for the design phase, as it is premised by the completion of the railway and the train. What is worse, both full-scale and reduced-scale tests have a high cost. With the development of computer hardware, numerical simulation has emerged as a cost-efficient method for design selection. For instance, Kozo Fujii [13] and Jenn-Long Liu [14] probed into the formation and regularity of the pressure wave in tunnel, respectively using the finite-difference method and the overlapping mesh method. In addition, many scholars [15~18] have applied commercial CFD software to simulate the formation of tunnel pressure waves and the impact of train shape and auxiliary tunnels. In general, numerical simulation methods can be divided into 1D methods, 3D methods and combination methods. The 3D methods can capture outside pressure distribution and other details features of the local pressure. Nonetheless, the tunnel length of 3D simulation is limited to 4km under the current hardware constraint. Relatively speaking, 1D flow models are good at quick comparison and selection of multiple parameters in the design phase. Until now, source programs [19-20] like ThermoTun and DB-TUNEL still play an important role in the selection of tunnel cross-sectional area and evaluation of the passenger comfort [21-22].

Through the above analysis, this paper studies the pressure fluctuations in the tunnel operation of two maglev trains using the 1D compressible unsteady non-homentropic flow model and the method of characteristics, aiming to determine the proper cross-sectional area for tunnels on high-speed maglev lines and optimize the airtightness design for high-speed maglev trains.

2. OVERVIEW OF 1D FLOW MODEL

When a high-speed maglev train passes through a tunnel, it will induce a 3D, compressible, unsteady, and turbulent flow. In general, the length of the tunnel is much greater than its hydraulic diameter. This geometrical feature allows the simplification of the 3D flow as 1D flow, except for the train ends and the tunnel entrance.

2.1 Governing equations

The target tunnel is a horizontal one with no abrupt changes in the cross-section or auxiliary structures like ventilation shaft. It is assumed that the train body is absolutely airtight with no exchange between inside and outside air, and that the air in the tunnel is ideal gas. Considering the friction and heat transfer between the air and the wall surface of the train or the tunnel, the governing equations for the 1D compressible non-homentropic flow model [20] can be established as:

Continuity equation:

$$\frac{\partial \rho}{\partial t}+u\frac{\partial \rho}{\partial x}+\rho\frac{\partial u}{\partial x}=0 \tag{1}$$

Momentum equation:

$$\frac{\partial u}{\partial t}+u\frac{\partial u}{\partial x}+\frac{1}{\rho}\frac{\partial p}{\partial x}+G=0 \tag{2}$$

Energy equation:

$$\left(\frac{\partial p}{\partial t}+u\frac{\partial p}{\partial x}\right)-a^2\left(\frac{\partial \rho}{\partial t}+u\frac{\partial \rho}{\partial x}\right)=\left(q-w+uG\right)\rho\left(\kappa-1\right) \tag{3}$$

where u and a are the air speed and the local sound speed, respectively; ρ, p and κ are density, pressure and specific heat ratio of the air, respectively; g is the gravity acceleration; w is the power of the moving wall surface on the air; G is the frictional item; q is the heat transfer item between the air and wall surface of the train or the tunnel; t is the time. The values of G, q and w are dependent on the relative position of train and tunnel.

(1) The flow in the empty tunnel with no trains in the duct can be expressed as:

$$G=\frac{S_{\mathrm{TU}}}{2F_{\mathrm{TU}}}f_{\mathrm{TU}}u|u| \tag{4}$$

$$q=\frac{S_{\mathrm{TU}}}{2F_{\mathrm{TU}}}\frac{\kappa R}{\kappa-1}f_{\mathrm{TU}}|u|\left(T_{\mathrm{TU}}-T\right) \tag{5}$$

$$w=0 \tag{6}$$

(2) When a single train runs through the tunnel, the flow in the annulus between the train and the tunnel can be expressed as:

$$G=\frac{1}{2F_{\mathrm{AN}}}\left\{f_{\mathrm{TU}}u|u|S_{\mathrm{TU}}+f_{\mathrm{TR}}(u-V)|u-V|S_{\mathrm{TR}}\right\} \tag{7}$$

$$\begin{aligned}q=&\frac{\kappa R}{2(\kappa-1)F_{\mathrm{AN}}}\left\{f_{\mathrm{TU}}|u|S_{\mathrm{TU}}\left(T_{\mathrm{TU}}-T\right)\right.\\&\left.+f_{\mathrm{TR}}|u-V|S_{\mathrm{TR}}\left(T_{\mathrm{TR}}-T\right)\right\}\end{aligned} \tag{8}$$

$$w=\frac{S_{\mathrm{TR}}}{2F_{\mathrm{AN}}}f_{\mathrm{TR}}V\left(u-V\right)|u-V|. \tag{9}$$

(3) When two trains run through the tunnel, the flow in the annulus between the tunnel and the two trains can be expressed as:

$$\begin{aligned}G=&\frac{1}{2F_{\mathrm{AN2}}}f_{\mathrm{TU}}u|u|S_{\mathrm{TU}}\\&+\frac{1}{2F_{\mathrm{AN2}}}f_{\mathrm{TR1}}\left(u-V_{\mathrm{TR1}}\right)|u-V_{\mathrm{TR1}}|S_{\mathrm{TR1}}\\&+\frac{1}{2F_{\mathrm{AN2}}}f_{\mathrm{TR2}}\left(u-V_{\mathrm{TR2}}\right)|u-V_{\mathrm{TR2}}|S_{\mathrm{TR2}}\end{aligned} \tag{10}$$

$$\begin{aligned}q=&\frac{1}{2F_{\mathrm{AN2}}}\frac{\kappa R}{\kappa-1}\left[f_{\mathrm{TU}}S_{\mathrm{TU}}|u|\left(T_{\mathrm{TU}}-T\right)\right.\\&+f_{\mathrm{TR1}}S_{\mathrm{TR1}}|u-V_{\mathrm{TR1}}|\left(T_{\mathrm{TR1}}-T\right)\\&\left.+f_{\mathrm{TR2}}S_{\mathrm{TR2}}|u-V_{\mathrm{TR2}}|\left(T_{\mathrm{TR2}}-T\right)\right]\end{aligned} \tag{11}$$

$$w = \frac{S_{\mathrm{TR1}}}{2F_{\mathrm{AN2}}} f_{\mathrm{TR1}} V_{\mathrm{TR1}} \left(u - V_{\mathrm{TR1}}\right) | u - V_{\mathrm{TR1}} | + \frac{S_{\mathrm{TR2}}}{2F_{\mathrm{AN2}}} f_{\mathrm{TR2}} V_{\mathrm{TR2}} \left(u - V_{\mathrm{TR2}}\right) | u - V_{\mathrm{TR2}} | \quad (12)$$

where F_{TU} and F_{AN} are the cross-sectional area of the tunnel and the annulus between the single train and the tunnel, respectively; S_{TU} and S_{TR} are the perimeters of the cross-section of the tunnel and the train, respectively; f_{TU} and f_{TR} are the friction coefficients of the tunnel and the train, respectively; R and V are gas constant and train speed, respectively; T and T_{TU} are the temperatures inside the tunnel and on the tunnel wall, respectively; subscripts 1 and 2 indicate whether the corresponding parameters belong to train #1 or train #2, except that F_{AN2} is the cross-sectional area of the annulus between the tunnel and two trains.

2.2 Boundary conditions

During the simulation with the 1D compressible flow model, the boundary conditions at the tunnel portals and train ends were described by a 1D quasi-steady non-homentropic flow model [20]. In fact, the flow at the boundary of tunnel portals and train ends is an unsteady 3D flow. However, the boundary region is extremely short compared with the entire tunnel. The flow parameters change more violently with the spatial distance x than with the time, that is, $\partial/\partial x >> \partial/\partial t$. It can be approximated that $\partial/\partial t = 0$, making it possible to assume the boundary flow as quasi-steady. The quasi-steady homentropic flow model and non-homentropic flow model have been implemented for boundary simulaitons, respectively [24, 25].

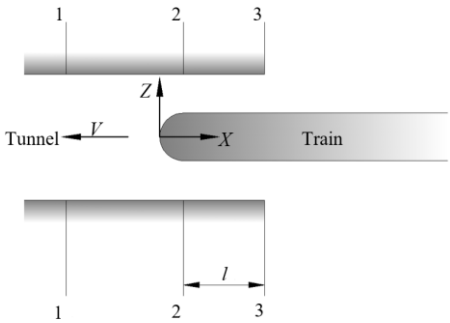

Figure 1. The entry of train nose

Taking the entry of train nose into the tunnel as an example (Figure 1), the reference coordinate system moving with the train was selected to establish the moving boundary conditions. Then, the relationship between the air speeds in the train coordinate system and the reference coordinate system can be defined as $u'=u-V$.

According to the governing equations and the formula of pressure-loss coefficient at the train nose, the boundary condition can be described as:

$$\rho_1 F_1 u_1' = \rho_2 F_2 u_2' \quad (13)$$

$$\left(p_2 - p_3\right) F_{\mathrm{AN}} - \tau_{\mathrm{TU}} l S_{\mathrm{TU}} - \tau_{\mathrm{TR}} l S_{\mathrm{TR}} = \left(\rho_3 u_3^2 - \rho_2 u_2^2\right) F_{\mathrm{AN}} \quad (14)$$

$$a_1^2 + \frac{\kappa - 1}{2} u_1'^2 = a_2^2 + \frac{\kappa - 1}{2} u_2'^2 = a_{01}'^2 = a_{02}'^2 \quad (15)$$

$$\zeta_{\mathrm{N}} = \frac{p_{01} - p_{02}}{\frac{1}{2}\rho_2 u_2'^2} = \frac{p_{01} - p_{02}}{\frac{1}{2}\frac{\kappa p_2}{a_2^2} u_2'^2} = \frac{p_{01} - p_{02}}{\frac{1}{2}\kappa p_2 \left(\frac{u_2'}{a_2}\right)^2} \quad (16)$$

where subscript 0 represents the stagnation state of the air; subscripts 1, 2 and 3 represent the flow parameters in Sections 1-1, 2-2 and 3-3, respectively; F is the flow area; u' is the air speed in train coordinate system; ζ_N is the pressure-loss coefficient at train nose. The control equations reflect the features of quasi-steady non-homentropic flow. The boundary conditions of the entry of train tail, the exit of train nose, and the exit of train tail can be established in a similar manner.

If two trains pass through the tunnel, the boundary conditions of the tunnel operation should be constructed for both trains. In light of the short crossing time, the air flow can be viewed as incompressible [26].

2.3 Simulation method

Equations (1)~(3) constitute a set of first-order, quasi-linear hyperbolic, partial differential equations, which can be solved by the method of characteristics. As an inverse marching method and the method of characteristics of generalized Riemann variables is adopted for our research. By this method, equations (1)~(12) were transformed into characteristic equations in u, ρ, and p, and then rewritten in dimensionless form using λ, β, and A_{A}, with λ and β being dimensionless generalized Riemann variables and A_{A} being the dimensionless entropy of air particles. In addition, the flow speed, length, sound speed and time were also introduced in dimensionless forms.

Considering the air flow in empty tunnel, the direction conditions and characteristic equations can be established as follows.

(1) Characteristic line of particle trajectory A_A:

Direction condition

$$\left(\frac{dX}{dZ}\right)_{A_{\mathrm{A}}} = U$$

Characteristic equation

$$\mathrm{d}A_{\mathrm{A}} = \delta A_{\mathrm{A}f} + \delta A_{\mathrm{A}h} \quad (17)$$

(2) Rightward characteristic line λ:

Direction condition

$$\left(\frac{dX}{dZ}\right)_{\lambda} = U + A$$

Characteristic equation

$$\mathrm{d}\lambda = \delta\lambda_{A_{\mathrm{A}}} + \delta\lambda_f + \delta\lambda_h \quad (18)$$

(3) Leftward characteristic line β

Direction condition

$$\left(\frac{dX}{dZ}\right)_{\beta} = U - A$$

Characteristic equation

$$\mathrm{d}\beta = \delta\beta_{A_A} + \delta\beta_f + \delta\beta_h \tag{19}$$

where subscripts A_A, f, and h represent the effects of gas entropy, friction and heat transfer on air flow, respectively. The impacts of these factors on λ, β and A_A can be expressed as:

$$\delta\lambda_{A_A} = \delta\beta_{A_A} = \frac{\lambda+\beta}{2}\frac{\mathrm{d}A_A}{A_A} \tag{20}$$

$$\left.\begin{matrix}\delta\lambda_f \\ \delta\beta_f\end{matrix}\right\} = \mp\frac{\kappa-1}{2}\left[1 \mp 2\frac{(\lambda-\beta)}{(\lambda+\beta)}\right]\frac{l_R}{a_R^2}G\mathrm{d}Z \tag{21}$$

$$\left.\begin{matrix}\delta\lambda_h \\ \delta\beta_h\end{matrix}\right\} = \frac{(\kappa-1)^2}{(\lambda+\beta)}\frac{(q-w)}{a_R^3}l_R\mathrm{d}Z \tag{22}$$

$$\delta A_{Af} = \frac{2(\lambda-\beta)}{(\lambda+\beta)^2 a_R^2}G\mathrm{d}Z \tag{23}$$

$$\delta A_{Ah} = \frac{2(\kappa-1)}{(\lambda+\beta)^2}\frac{(q-w)}{a_R^3}l_R\mathrm{d}Z \tag{24}$$

where l_R is reference length; a_R is reference sound speed; Z is the dimensionless time.

Following the method of characteristics of generalized Riemann variables, the λ, β and A_A at time Z_2 can be solved as:

$$A_{A2} = A_{A1} + \mathrm{d}A_A \tag{25}$$

$$\lambda_2 = \lambda_1 + \mathrm{d}\lambda \tag{26}$$

$$\beta_2 = \beta_1 + \mathrm{d}\beta \tag{27}$$

Finally, λ, β and A_A can be transformed to u, ρ, and p. The detailed steps are as follows:

(1) Define the physical model and geometrical parameters.
(2) Define the initial state and boundary conditions.
(3) Define the dimensionless parameters.
(4) Determine the grid length ΔX.
(5) Determine the λ, β and A_A of all grid points at time Z.
(6) Calculate the time step of each grid point by the stability criterion, and take the minimum value.
(7) Determine the flow direction, the position of interpolation points and the λ, β and A_A.
(8) Calculate the A_A. of the target point at time Z+ΔZ by the characteristic equation of particle trajectory.
(9) Calculate the λ and β of the target point at time Z+ΔZ by the characteristic equations of λ and β.
(10) Determine the unknown λ, β and A_A of boundary grid points by the boundary conditions.
(11) Calculate the flow parameters (i.e. gas pressure, speed, temperature and density) of each grid point by the relations of the generalized Riemann variables and the thermodynamic relations.
(12) Assign the λ, β and A_A of each grid point at time Z+ΔZ to the grid point at time Z .
(13) Repeat Steps (6) to (12) unless reaching the required computing time.
(14) Terminate the program.

2.4 Validation

The current speed record of high-speed maglev train stands at 500 km/h. However, there is not yet an agreed test speed for high-speed maglev trains. Here, the results of the moving model rigs in Japan [19] are used to validate our model. Specifically, the tunnel length was set to 14.7 m; the tunnel diameter was set to 0.1 m; the distance between the pressure transducer and the entrance was set to 2.35 m. It is assumed that the tunnel has a uniform cross-section. The transducer placement ensures that the device is far away from the obvious 3D flow area at the entrance. This area has been studied in great details in previous research [27, 28].

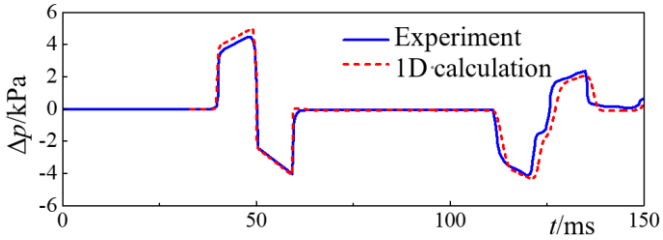

(a) Pressure fluctuations at 2.35 m from the entrance

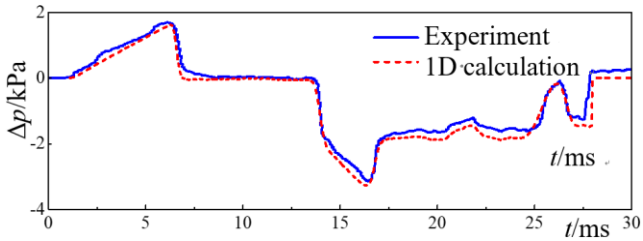

(b) Pressure fluctuations outside the train

Figure 2. Comparison between the results of our model and the moving model rigs and full-scale test

As shown in Figure 2(a), the pressure fluctuations at 2.35m form the entrance calculated by our model were the same with as those obtained by the moving model rigs, indicating that our model can predict the exact pressure fluctuations when the train passes through the tunnel at a speed up to 500 km/h. The maximum errors of the positive and negative pressures were 8.5 % and 1.8 %, respectively, which may be attributed to the effect of aerodynamic coefficients in our model.

After verifying the pressure fluctuations in the tunnel, an additional verification was performed to check the prediction accuracy of pressure fluctuations outside the train (Figure 2(b)). A full-scale test was carried out at the 2,818 m Xikema #1 Tunnel on Beijing-Shanghai High-Speed Railway with a CRH380AL train. The test speed was 380km/h. It is clear that the results of our model agreed well with those of the full-scale test, and the maximum errors of the positive and negative pressures were -3.9 % and 4.1 %, respectively. To sum up, the flow model is proved feasible for subsequent analysis.

3. INFLUENCING FACTORS ANALYSIS

Previous studies have shown that the pressure fluctuations outside the train are much higher in the tunnel operation of two trains than that of a single train. The pressure fluctuations is particularly pronounced at the centre of the tunnel at the same train speed.

In Figures 3(a) and 3(c), the thick solid line and thick dash line represent the track of train nose and that of train tail, respectively; the thin solid line and thin dash line represent that track of compression wave (CW) and that of expansion wave (EW), respectively. Figure 3 (b) compares the time histories of pressure fluctuations at train nose between single-train and two-train operations.

As shown in Figure 3, it is easy to see that the front of the compression wave produced by the entry of train 2# did not reach the nose of train 1# before 1.18 s; in this period, the pressure fluctuations were identical to those in single-train operation. At t = 1.18 s, the nose pressure rocketed up under the compression wave. When the two trains met, the pressure plunged deeply, and fluctuated far more violently than the single-train operation.

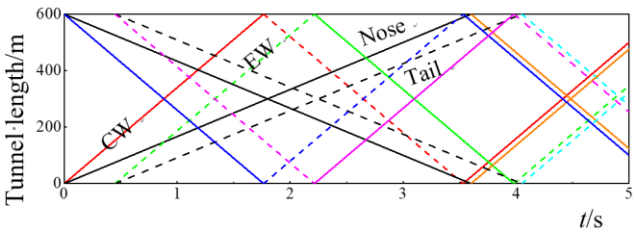

(a) Two–train operation

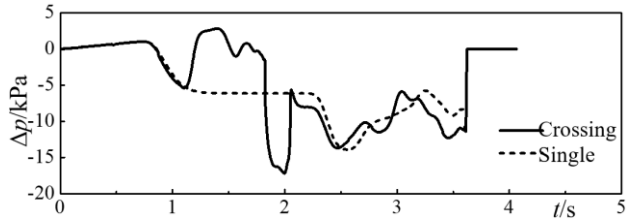

(b) Time history of pressure fluctuations at train nose

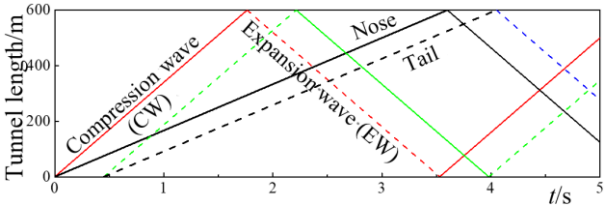

(c) Sing-train operation

Figure 3. Time histories of pressure fluctuations in different cases

Table 1 lists the maximum positive pressure variation (Δp_{max}+), the maximum negative pressure variation (Δp_{max}-) and peak-to-peak values. The statistics in the table reveal that, in the two-train operation, the Δp_{max}^{+} grew by 167.9 %, and the peak-to-peak value increased by 33.6 %.

The pressure variation at 3.6 s is resulted from the exit of train nose. At this moment, the pressure at the train nose suddenly restored to the ambient pressure. The variation depends on the pressures before and after the exit of train nose. Compared to the single-train operation, two-train operation always has a high negative pressure before the exit of train nose. The post-exit pressure is the ambient pressure. The pressure variation at 3.6 s was very obvious, as the reflected expansion wave affected the train nose at about 3.5s.

Table 1. Maximum pressure variation

	Δp_{max}+ /kPa	Δp_{max}- /kPa	Peak-to-peak /kPa
Single-train operation	1.06	-13.94	15.00
Two-train operation	2.84	-17.19	20.03
Increment	167.9%	23.4%	33.6%

In actual operations, it is impossible to eliminate the extreme condition that two trains moving at the same speed met at the centre of the tunnel (hereinafter referred to as the extreme condition). This condition should not be overlooked in the train design. Hence, the following sections attempt to discuss the influencing factors on this condition.

3.1 Effect of tunnel length

Inspired by previous research [29], the critical tunnel length derived from the Δp_{max}- at train tail in the extreme condition is:

$$L_{TU,crit} = \frac{L_{TR}}{M_{TR}} \tag{28}$$

According to the superposition and reflection laws of compression wave and expansion wave, the critical tunnel length derived from the Δpmax- at train nose is:

$$L_{TU,crit} = \begin{cases} \dfrac{L_{TR}}{M_{TR}} & M_{TR} \le \dfrac{1}{3} \\ \dfrac{2L_{TR}}{1 - M_{TR}} & M_{TR} > \dfrac{1}{3} \end{cases} \tag{29}$$

The above equations show the positive correlation between the critical tunnel length and the train length; the critical tunnel length based on the Δp_{max}- decreased with the increase of the train speed, while that based on the Δp_{max}^{+} at train nose decreased when the train speed was slower than 1/3 Mach and increased when the train speed was greater than that value. In the extreme condition, the critical tunnel length fell in [150 m, 1,050 m] for 75 m, 125 m and 250 m-long high-speed maglev trains.

Figure 4 shows relationship between tunnel length and Δp_{max}+, Δp_{max}- and the peak-to-peak value of 75m-long high-speed maglev trains. Here, the predicted tunnel length ranges from twice the train length to 2km. The cross-sectional area of the tunnel was set to 100 m^2 according to the wheel-rail system in China, and the train speed was set to 500 km/h. It can be seen from Figure 4 that the Δp_{max}+ , Δp_{max}- and peak-to-peak value remained basically the same in the tunnel longer than 400 m, 750 m and 750 m, and only decreased slowly with the increase of tunnel length. For other train lengths, the peak values all remained unchanged when the tunnel length was more than 4 times of the critical tunnel length.

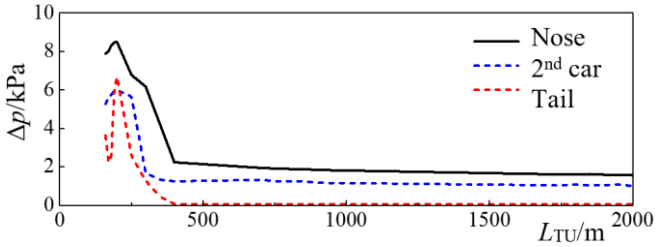

(a) Relationship between Δp_{max}+ at train nose and tunnel length

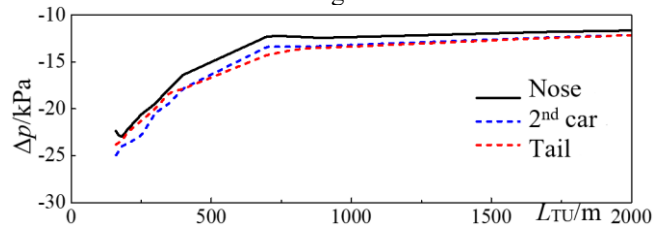

(b) Relationship between Δp_{max}- at train tail and tunnel length

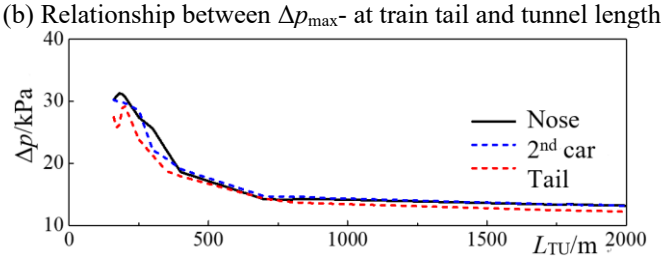

(c) Relationship between peak-to-peak value at train tail and tunnel length

Figure 4. Effect of tunnel length on maximum pressure variation

Table 2. Critical tunnel lengths

Train speed /kmh^{-1}	Based on Δp_{max}+ /m			Based on Δp_{max}- /m		
	75m	125m	250m	75m	125m	250m
400	250	400	800	220	340	600
450	220	340	700	160	280	700
500	200	350	750	160	300	550
550	200	360	800	160	260	510
600	200	380	850	160	260	510
650	220	420	950	160	260	510

Table 2 lists the critical tunnel lengths obtained through our 1D predictions. It is clear that the trends with train length and speed are almost the same as the results of equations (28) and (29), which were deduced from the superposition and reflection laws of compression wave and expansion wave. In addition, the results of our simulation agree well with those in Reference [29]. All these demonstrate that the critical tunnel lengths based on the Δp_{max}+ at train nose are rational, despite the lack of full-scale or reduced-scale data. Hence, the data in Table 2 are adopted for the subsequent analysis.

3.2 Effect of tunnel cross-sectional area

Figure 5 shows relationship between tunnel cross-sectional area and Δp_{max}+, Δp_{max}- and the peak-to-peak value of the 125m-long high-speed maglev trains in the extreme condition. Using the critical tunnel lengths in Table 2, Figures 5(a) and (b) are plotted with the recommended 5.5kPa threshold for the absolute maximum pressure variation in Germany.

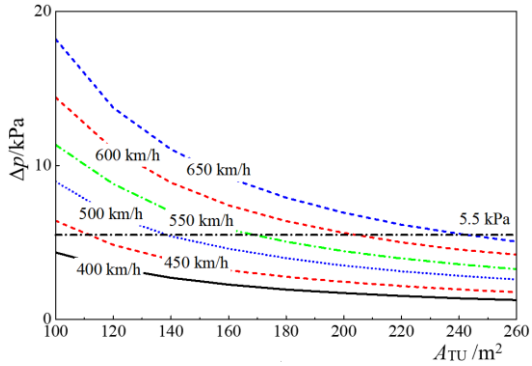

(a) Relationship between Δp_{max}+ at train nose and tunnel cross-sectional area

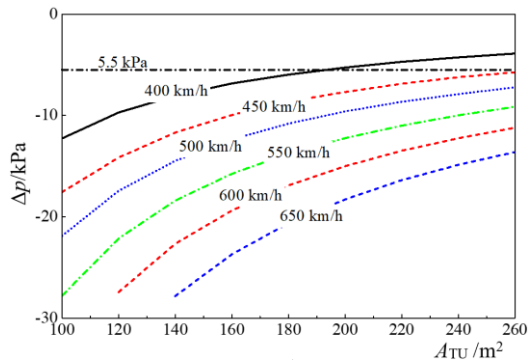

(b) Relationship between Δp_{max}- at train tail and tunnel cross-sectional area

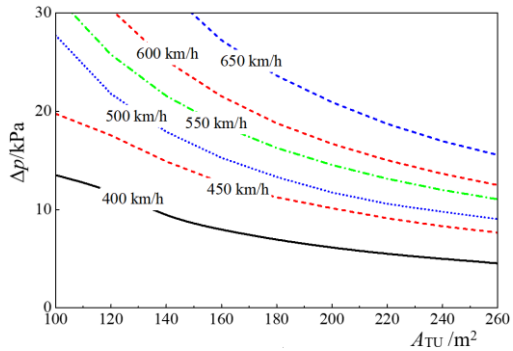

(c) Relationship of peak-to-peak value at train tail and tunnel cross-sectional area

Figure 5. Effect of tunnel cross-sectional area on maximum pressure variation

As can be seen from Figure 5, Δp_{max}+, Δp_{max}- and the peak-to-peak value all decreased with the increase of tunnel cross-sectional area. Under the Germany criterion, the train can only be operated under 400 km/h and the tunnel cross-sectional area should not be smaller than 193 m^2, which far beyond the largest available area of 107 m^2 in the world.

Table 3. Exponents for different tunnel sectional areas

Tunnel cross-sectional area/m^2	*n* for Δp_{max}+	*n* for Δp_{max}-	*n* for peak-to-peak value
100	2.80	2.25	2.55
140	2.72	2.36	2.15
180	2.68	2.37	2.08
220	2.67	2.36	2.04
260	2.68	2.36	2.02

It is found that Δp_{max}+, Δp_{max}- and the peak-to-peak value can be well fitted with tunnel cross-sectional area by

exponential function. Table 3 lists the exponent n for different tunnel sectional areas. It is found that the range of n for $\Delta p_{max}+$, $\Delta p_{max}-$ and the peak-to-peak value was -1.3 ~ -1.4, -1.1 ~ -1.2 and -1.0 ~ -1.2, respectively.

3.3 Effect of train speed

Figure 6 describes the relationship between train speed and $\Delta p_{max}+$, $\Delta p_{max}-$ and the peak-to-peak value of 125 m-long high-speed maglev trains in the extremely condition.

The aforementioned critical tunnel lengths were also used in this section. The cases for 75 m- and 250 m-long trains are omitted because they share the same trend with the case of 125 m-long trains. It can be inferred from Figure 6 that $\Delta p_{max}+$, $\Delta p_{max}-$ and the peak-to-peak value all increased with the train speed.

It is also found that $\Delta p_{max}+$, $\Delta p_{max}-$ and the peak-to-peak value can be well fitted with train speed by exponential function. Table 3 lists the exponent n for different train speeds. It is found that the range of n for $\Delta p_{max}+$, $\Delta p_{max}-$ and the peak-to-peak value was 2.7 ~ 2.8, 2.3 ~ 2.4 and 2.0 ~ 2.6, respectively.

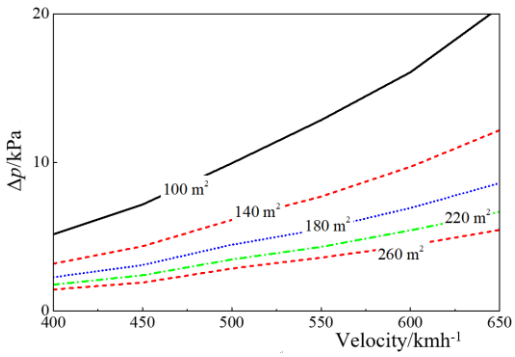

(a) Relationship between $\Delta p_{max}+$ at train nose and train speed

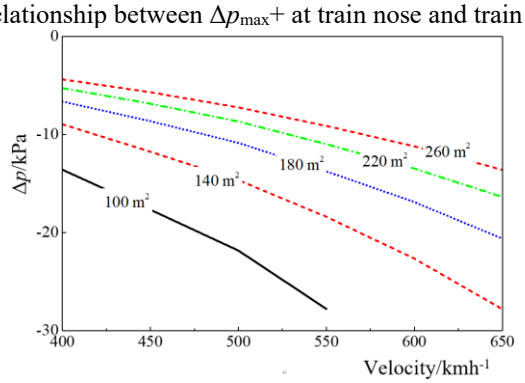

(b) Relationship between $\Delta p_{max}-$ at train tail and train speed

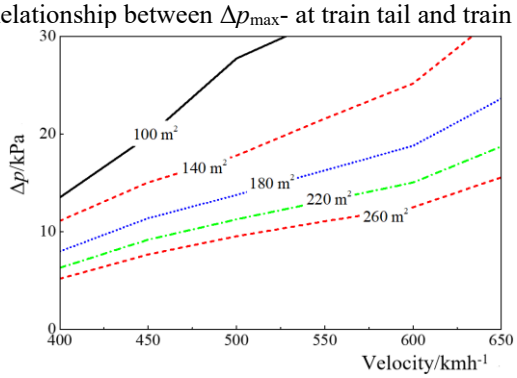

(c) Relationship between peak-to-peak value at train tail and train speed

Figure 6. Effect of train speed on maximum pressure variation

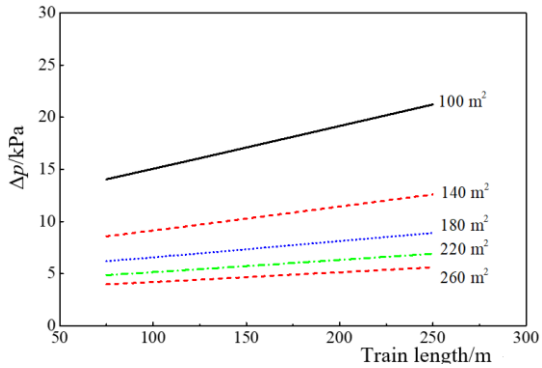

(a) Relationship between $\Delta p_{max}+$ at train nose and train length

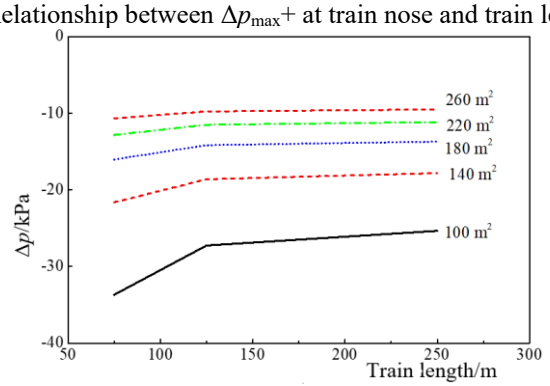

(b) Relationship between $\Delta p_{max}-$ at train tail and train length

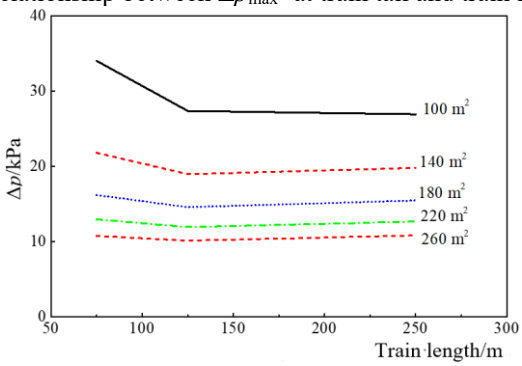

(c) Relationship between peak-to-peak value at train tail and train length

Figure 7. Effect of train length on maximum pressure variation

Table 4. Exponents for different train speeds

Train speed /kmh^{-1}	n for $\Delta p_{max}+$	n for $\Delta p_{max}-$	n for peak-to-peak value
400	-1.33	-1.21	-1.17
450	-1.38	-1.19	-1.00
500	-1.33	-1.18	-1.21
550	-1.34	-1.17	-1.12
600	-1.34	-1.16	-1.16
650	-1.38	-1.16	-1.20

3.4 Effect of train length

Figure 7 depicts the relationship between train length and $\Delta p_{max}+$, $\Delta p_{max}-$ and the peak-to-peak value in the extreme condition. The aforementioned critical tunnel lengths were also used in this section. As shown in Figure 7, $\Delta p_{max}+$ increased with the train length, while $\Delta p_{max}-$ and the peak-to-peak value increased firstly and then remained almostly unchanged with the increase of train length.

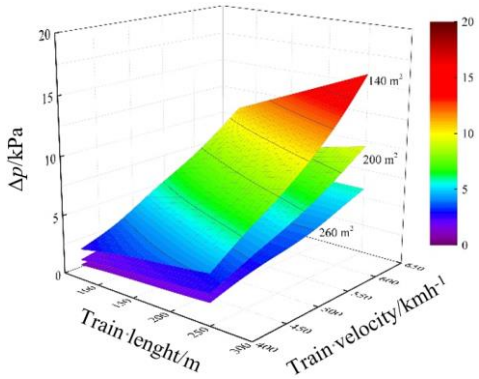

(a) Effect on Δp_{max}+ at train nose

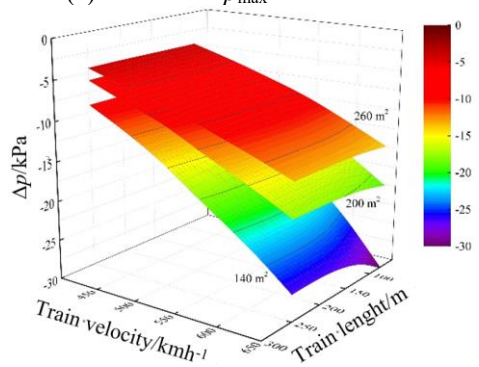

(b) Effect on Δp_{max}- at train tail

Figure 8. Coupled effect of train speed and train length on maximum pressure variation

Figure 8 illustrates the coupled effect of train speed and train length on maximum pressure variations at train nose and train tail. The cross-sectional area of the tunnel was 140m^2, 200 m^2 and 260 m^2 respectively. It is clear that the train speed and train length are positively correlated with the Δp_{max}+ at train nose and the Δp_{max}- at train tail.

4. CONCLUSIONS

This paper investigates the pressure waves produced by the tunnel operation of two maglev trains moving at the speed up to 650 km/h, using 1D compressible unsteady non-homentropic flow model and the characteristic method for generalized Riemann variables. The simulation results were compared to those from the reduced-scale test in Japan and full-scale test in China. The comparison proves that our 1D model is a rational and efficient tool for pressure wave prediction. Through repeated computations of the 1D model, the critical tunnel lengths were obtained. Then, the author explored the effects of tunnel length, tunnel cross-sectional area, train speed and train length on maximum pressure variation. The preliminary conclusions are as follows:

First, the critical tunnel lengths obtained by the 1D model based on the Δp_{max}+ range of 160 m ~ 950 m agree well with those in Reference [29], in which the range is 150 m~1,050 m. In addition, the critical tunnel length based on the Δp_{max}+ is longer than that based on the Δp_{max}- .

Second, the tunnel cross-sectional area, and train speed have greater impacts than the train length on the Δp_{max}+ and the Δp_{max}- of the train. The peak pressure change of the train is about -1.1 ~ -1.4 times the tunnel cross-sectional area, and 2.0 ~ 2.7 times the train speed.

Third, under the German threshold criterion of 5.5 kPa, the cross-sectional area is up to 193 m^2 in the extreme condition that two 125m-long trains passing at 400 km/h. Therefore, special attentions should be paid to the presence of 150~1,000m-long tunnels on high-speed maglev lines. To prevent blocking the effect, a possible solution is to increase the tunnel length to 4 times the critical length.

Fourth, the research results indicate that for the severe pressure fluctuations inducted by two crossing maglevs in the tunnel, double-tube single-track tunnel type should be pay more attentions in the high-speed maglev lines instand of single-tube double-track tunnel type.

ACKNOWLEDGMENT

The authors would like to thank the support provided by the National Key Research and Development Program of China (2016YFB1200602-39) and Youth Science Fund Project of Lanzhou Jiaotong University (2017010).

REFERENCES

[1] Masahiro S, Shiro H, Takamasa I, Katsuya Y, Naoto T. (2003). Summary of running test results of new vehicles for Yamanashi Maglev Test Line. Transactions of the JSME 15: 305-308.

[2] Kazuya T, Atsushi H, Kojiro N, Tetsuya D, Takanobu O. (2015). Reduction of a micro-pressure wave by a round hood at a tunnel portal of a high-speed railway. Jsce Earthquake Engineering Symposium 71(2): 167-172. https://doi.org/10.2208/jscejseee.71.167

[3] Atsushi H, Kazuya T, Kojiro N, Tetsuya D, Takanobu O, Masanobu I, Yozo F. (2015). Proposal of a porous hood for a high-speed railway tunnel based on an evaluation of a micro-pressure wave. Jsce Earthquake Engineering Symposium 71(3): 327-340. https://doi.org/10.2208/jscejseee.71.327

[4] Atsushi H, Kazuya T, Kojiro N, Tetsuya D, Takanobu O, Masanobu I, Yozo F. (2015). Distortion of compression wave propagating through a long tunnel of high-speed railway and reduction of micro-pressure wave using a portal hood. Jsce Earthquake Engineering Symposium 71(1): 128-138. https://doi.org/10.2208/jscejseee.71.128

[5] Saito T. (2015). Research on tunnel pressure fluctuation and tunnel micro pressure wave in high speed railroad, Osaka, Osaka University graduate school of engineering.

[6] Mikio Y, Toshihiro W, Takaaki N, Makoto U, Yozo F. (2003). Evaluation of pressure fluctuation in high-speed train tunnel. Japan Society of Civil Engineers (738): 171-189. https://doi.org/10.2208/jscej.2003.738_171

[7] Mikio Y, Satoru K, Toshihiro W, Masato O, Makoto U, Yozo F. (2004). Design of a tunnel lining versus pressure fluctuation in high-speed train tunnel. Proceedings of the Japan Society of Civil Engineers (752): 119-131. https://doi.org/10.2208/jscej.2004.752_119

[8] Kazuya K, Nobuharu M. (1993). Experimental study of the air pressure transients generated by the high speed trains passing through tunnels. Japan Society of Civil Engineers (458): 137-145. https://doi.org/10.2208/jscej.1993.137

[9] Tielkes TH. (2006). Aerodynamic Aspects of Maglev Systems, The 19th International Conference on

Magnetically Levitated Systems and Linear Drives, Dresden, Germany, 1-9.
[10] Zhang GP, Lei B, Li Q. (2005). influence of maglev train sealing characters on the tunnel cross-section area. Journal of The China Railway Society 27(2): 126-129.
[11] Zhang ZJ, Gao B, Wang YX. (2005). Study of propagation pattern of pressure waves produced by magnetically levitated train passing a tunnel. Journal of Shijiazhuang Railway Institute 18(4): 11-14.
[12] Liu CQ, Peng HJ. (2011). Study of Tunnel Clearance Area and Inner Perimeter of Magnetic Levitation Railways. Modern Tunnelling Technology 48(4): 39-43.
[13] Fujii K, Takanobu O. (1995). Aerodynamics of high speed trains passing by each other. Computers & Fluids 24(8): 897-908. https://doi.org/10.1016/0045-7930(95)00024-7
[14] Liu JL. (2004). Computations of two passing-by high-speed trains by a relaxation overset-grid algorithm. International Journal for Numerical Methods in Fluids 44(12): 1299-1315. https://doi.org/10.1002/fld.631
[15] Tian HQ. (2007). Aerodynamics of Train. China Railway Publishing House.
[16] Gilbert T, Baker C, Quinn A. (2013). Aerodynamic pressures around high-speed trains: the transition from unconfined to enclosed spaces. Proceedings of the Institution of Mechanical Engineers, Part F: Journal of Rail and Rapid Transit 227(6): 609-622. https://doi.org/10.1177/0954409713494947
[17] Li RX, Yuan L. (2014). Pressure waves in tunnels when high-speed train passing through, Journal of Mechanical Engineering 50(24): 115-121. https://doi.org/10.3901/JME.2014.24.115
[18] Yang GW, Wei YJ, Zhao GL, Liu YB, Zhang YY, Xing YL, Zeng XH, Lai J, Han W, Chen QS, Liu QS, Li JC, Hu KX, Yang ZP, Liu WZ, Wang WJ, Sun SG, Zhang WH, Zhou N, Lv QS, Li RP, Jin XS, Wen ZF, Xiao XB, Zhao X, Cui D, Wu B, Zhong SQ, Zhou X. (2015). Research on key mechanics of high - speed train. Progress in Mechanics 45(7): 217-460. https://doi.org/10.6052/1000-0992-13-091
[19] Saito S, Iida M, Kajiyama H. (2011). Numerical simulation of 1-D unsteady compressible flow in railway tunnels. Journal of Environment and Engineering 6(4): 723-738. https://doi.org/10.1299/jee.6.723
[20] Mei YG, Zhou CH, Xu JL. (2009). Aerodynamics of high-speed Railway Tunnel. Science Press, Beijing.
[21] Wormstall-Reitschuster HJ, Gatschke G. (2000) Parametrical investigations on aerodynamic effects in tunnels-prediction and validation. 10th Inter. Symposium on Aerodynamics, Ventilation & Fire in Tunnels, BHRA, 171-183.
[22] Vardy A. (2013). Fuzzy criteria for pressure comfort in tunnels. 15th Inter. Symposium on Aerodynamics, Ventilation & Fire in Tunnels, 525-538.
[23] Yu NY, Mei YG. (2003). Study on main parameters effecting pressure transients while train passing through tunnel. China Railway Science 24(6): 67-69.
[24] Fox JA, Vardy AE. (1973). The generation and alleviation of air pressure transients caused by the high speed passages of vehicles through tunnels. Stephens H. S. 1st Inter. Symposium on Aerodynamics, Ventilation & Fire in Tunnels, Cranfield 3: 49-64.
[25] Pope CW, Woods WA. (1982). Boundary conditions for the transit of a train through a tunnel with special reference to the entry and exit mesh fractions and the contact surface. Stephens H.S. 4th Inter. Symposium on Aerodynamics, Ventilation & Fire in Tunnels. Cranfield C1: 79-105.
[26] Steinrück P, Sockel H. (1985). Further calculations on transient pressure alleviation and simplified for initial tunnel design. 5th International Symposium on the Aerodynamics and Ventilation of Vehicle Tunnels, Cranfield E4: 317-342.
[27] Liu XX, Guo AN, Mei YG, Xu JL, Li SA, Zhou CH. (2015). Numerical simulation of pressure wave characteristics generated by a high-speed train passing through a double-track tunnel. Journal of Railway Science & Engineering 12(1): 20-27.
[28] Zhang XY. (2007). Aerodynamic load study on the high-speed railway tunnel. Chengdu: Southwest Jiaotong University, 41-56.
[29] CEN. (2006). Railway applications - Aerodynamics - Part5: Requirements and test procedures for aerodynamics in tunnels.

NOMENCLATURE

a	local sound speed, m.s^{-1}
A	dimensionless local sound speed
A_A	dimensionless entropy of air particles
f	friction coefficient
F	cross-sectional area, m^2
G	frictional iterm
l	the length of train entry the tunnel, m
L	length, m
M	Mach number
p	air pressure, Pa
q	heat transfer item between the air and thwall surface of the train or the tunnel
R	gas constant
S	perimeter, m
T	tempratures, K
t	time, s
u	air flow rate, m.s^{-1}
U	dimensionaless air flow rate
V	train speed, m.s^{-1}
w	power of the moving wall surface on the air
x	independent variable
X	dimensionaless x
Z	dimensionaless t

Greek symbols

β	Generalized Riemann variable with leftward characteristic line
Δ	change amount
κ	specific heat ratio of the air
λ	Generalized Riemann variable with rightward characteristic line
ρ	air density, kgm^{-3}
ξ	pressure-losse coefficient
τ	Shear force act on the train surface

Subscripts

0	stagnation state
1	parameter at section 1-1

1D	one-dimensional
2	parameter at section 2-2
3	parameter at section 3-3
3D	three-dimensional
A_A	effect of gas entropy
AN	annula with a single trian
AN2	annula with two trians
crit	critical length
CW	compression wave
EW	expansiona wave
h	effect of heat transfer
f	effect of friction
max	maximum
min	minimum
N	train nsoe
R	reference
TR	train
TR1	train #1 at corssing case
TR2	train #2 at corssing case
TU	tunnel
+	positive pressure variation
-	negative pressure variation